DOI:10.16555/j.1006-8775.2015.02.010

Article ID: 1006-8775(2015) 02-0194-17

THE IMPACT OF DIFFERENT PHYSICAL PROCESSES AND THEIR PARAMETERIZATIONS ON FORECAST OF A HEAVY RAINFALL IN SOUTH CHINA IN ANNUALLY FIRST RAINING SEASON

ZHANG Xu-bin (张旭斌)[1, 2], WAN Qi-lin (万齐林)[1, 2], XUE Ji-shan (薛纪善)[2, 3],
DING Wei-yu (丁伟钰)[1, 2], LI Hao-rui (李昊睿)[1, 2]

(1. Guangdong Provincial Key Laboratory of Regional Numerical Weather Prediction, CMA, Guangzhou 510080 China; 2. Institute of Tropical and Marine Meteorology, CMA, Guangzhou 510080 China; 3. Chinese Academy of Meteorological Sciences, Beijing 100081 China)

Abstract: An ensemble prediction system based on the GRAPES model, using multi-physics, is used to discuss the influence of different physical processes in numerical models on forecast of heavy rainfall in South China in the annually first raining season (AFRS). Pattern, magnitude and area of precipitation, evolution of synoptic situation, as well as apparent heat source and apparent moisture sink between different ensemble members are comparatively analyzed. The choice of parameterization scheme for land-surface processes gives rise to the largest influence on the precipitation prediction. The influences of cumulus-convection and cloud-microphysics processes are mainly focused on heavy rainfall; the use of cumulus-convection parameterization tends to produce large-area and light rainfall. Change in parameterization schemes for land-surface and cumulus-convection processes both will cause prominent change in forecast of both dynamic and thermodynamic variables, while change in cloud-microphysics processes show primary impact on dynamic variables. Comparing simplified Arakawa-Schubert and Kain-Fritsch with Betts-Miller-Janjic schemes, SLAB with NOAH schemes, as well as both WRF single moment 6-class and NCEP 3-class with simplified explicit schemes of phase-mixed cloud and precipitation shows that the former predicts stronger low-level jets and high humidity concentration, more convective rainfall and local heavy rainfall, and have better performance in precipitation forecast. Appropriate parameterization schemes can reasonably describe the physical process related to heavy rainfall in South China in the AFRS, such as low-level convergence, latent heat release, vertical transport of heat and water vapor, thereby depicting the multi-scale interactions of low-level jet and meso-scale convective systems in heavy rainfall suitably, and improving the prediction of heavy rainfall in South China in the AFRS as a result.

Key words: numerical weather prediction; heavy rainfall in South China in annually first raining season; GRAPES model; multi-physics; parameterization; ensemble prediction

CLC number: P457.8 **Document code:** A

1 INTRODUCTION

Heavy rainfall in South China in annually first raining season (from April to June) (hereafter AFRS), especially in the warm sector, is characterized by high frequency, large intensity and short duration, and is accompanied by thunderstorm usually. AFRS is the product of interactions among weather systems at different scales. On the one hand, intensive mesoscale convective systems (MCS) play an important role in the formation of AFRS (Sun and Zhao[1]; Meng et al.[2]; Zhang and Ni[3]; Zhang and Zhang[4]); on the other hand, AFRS is greatly influenced by synoptic scale weather systems, such as low-level jet (Liu et al.[5]), Southwest Vortex (He and Sun[6]) and shear line (Chen and Zhao[7]), as well as complex terrain (Sun et al.[8]). Therefore, for the purpose of improving the numerical weather prediction (NWP) of AFRS, a numerical model needs to include the multi-scale interactions among different weather systems related to AFRS as much as possible.

Heavy rainfall forms and develops through physical processes in the atmosphere, including processes in land surface, planetary boundary layer (PBL), cloud and rain. In addition to rugged terrain, land surface is also covered by different kinds of vegetation. As a result, there are complex interactions between the land surface and the atmosphere. Specifically, through exchange of both heat and vapor, land surface exerts important forcing on MCS related to heavy rainfall. Located between under-

Received 2014-10-30; **Revised** 2015-03-13; **Accepted** 2015-04-15

Foundation item: National Natural Science Foundation of China (41405104); Specialized Project for Public Welfare Industries (Meteorological Sector) (GYHY201306004); Guangdong Science and Technology Planning Project (2012A061400012); Project of Guangdong Provincial Meteorological Bureau for Science and Technology (2013A04); Science and Technology Plan for the 12th Five-Year of Social and Economic Development (2012BAC22B00)

Biography: ZHANG Xu-bin, Ph. D., associate researcher, primarily undertaking research on data assimilation, ensemble forecast and meso- and fine-scale numerical simulation.

Corresponding author: ZHANG Xu-bin, e-mail: xbzhang@grmc.gov.cn

lying surface and free atmosphere, PBL is responsible for the flux of heat, vapor and momentum from underlying surface in the whole atmosphere. Consequently, physical processes in PBL, including exchange and transport of heat, vapor and momentum among land surface, free atmosphere and MCS by eddy transports, make an impact on formation and development of heavy rainfall. Precipitation particles, such as rain, snow and ice, form through various different microphysical processes. As a consequence, the time, location and intensity of precipitation are not only affected by large-scale dynamical circulation, but also closely related to microphysical processes in cloud. Besides, precipitation can influence the dynamical and thermodynamical conditions of the environment, as well as the hydrometeorological cycle, through latent heat release, hydrometeorological transformation and loading; and the influenced environment will further influence the development of precipitation. Thus it can be seen that, whether NWP can well predict the formation and development of heavy rainfall or not largely depends on whether it can well depict various different physical processes associated with heavy rainfall.

Owing to the finite temporal and spatial resolution in numerical models, there are many important physical processes in the atmosphere that cannot be explicitly resolved by numerical models. Therefore, a method called "parameterization" is needed to describe these unresolved physical processes in numerical models. For one physical process, there is often more than one scheme that can be selected to do the corresponding parameterization. Due to differences of theoretical basis or empirical hypothesis in different parameterization schemes, there are also differences in corresponding forecasting result of numerical models using different schemes. Many previous works have shown that, different parameterization schemes have different impact on the location and intensity of rainfall in mesoscale numerical models (Wand and Seaman[9]; Gallus[10]; Gu[11]; Wang et al.[12]; Wang [13]; Jankov et al.[14, 15]; Zhang et al.[16]; Xue et al.[17]; Wu et al.[18]; Li et al.[19]; Sun et al.[20]; Liao et al.[21]). Both Wang and Seaman[9] and Gallus[10] found that, selection of cumulus parameterization scheme had great effect on the prediction of rainfall pattern. By comparing different parameterization schemes for different physical processes, Jankov et al.[14] indicated that the performance of NWP for precipitation was most sensitive to the change of cumulus parameterization scheme. For light rainfall, sensitivity of prediction performance to the change of PBL parameterization scheme was close to that of the change of microphysics parameterization scheme; while for heavy rainfall, prediction performance was more sensitive to the change of microphysics parameterization scheme. For rainfall in Guizhou province in the raining season, Wu et al. [18] conducted NWP experiments with the GRAPES model. The corresponding results showed that, there is larger influence of changing scheme on prediction performance for cumulus parameterization than for microphysics parameterization. Although the weather systems related to AFRS have the characteristics of multi-scale interactions, not all the combinations of different parameterization schemes for different physical processes can well depict these characteristics in numerical models. Using the WRF model, Liao et al.[21] conducted simulation experiments for a heavy rainfall in Pearl River Delta. Their results showed that, when the WSM6 (KF) scheme is used for microphysics (cumulus) parameterization, choosing the KF (Lin) scheme for cumulus (microphysics) parameterization can simulate the heavy rainfall more accurately than with other combinations. Accordingly, in order to improve the performance of NWP for AFRS, it is very necessary to understand the influence of different parameterization schemes on it.

Focusing on a case of AFRS, this study discussed the impact of different physical processes and their parameterizations on the performance of NWP for AFRS, based on an ensemble prediction system (EPS) using multi-physics with the GRPAES model.

2 OVERVIEW OF THE CASE AND EXPERIMENT DESIGN

2.1 *Case overview*

During 15-16 May 2013, under the effect of warm and wet air, a heavy rainfall event occurred in Guangdong province. In this event, heavy rain to rainstorm occurred, with torrential rain in some local areas. Thereinto, a rainstorm was concentrated in the north of Guangdong (such as Qingyuan Shaoguan, and Heyuan). The 24-h accumulated rainfall located at Fogang from 0000 UTC 15 to 0000 UTC 16 May reached 292.4 mm (Fig. 1), which is the largest precipitation amount in the whole province.

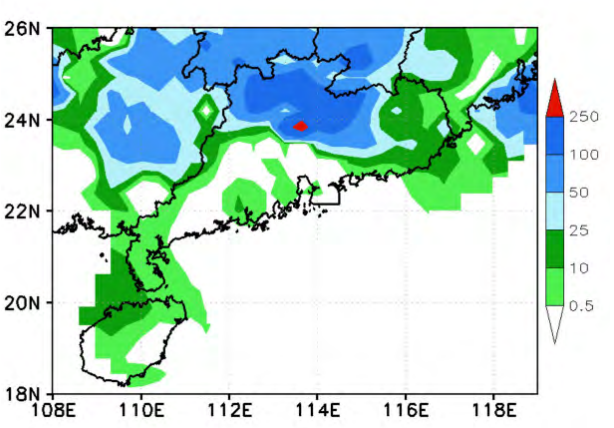

Figure 1. 24-h accumulated observed rainfall (unit: mm) from 0000 UTC 15 May to 0000 UTC 16 May 2013.

From 0000 UTC 15 (Fig.2a) to 0000 UTC 16 (Fig. 2b), a low vortex moved east gradually and then into the sea. During this process, a southwest low-level jet, especially the mesoscale core, at the east side of the

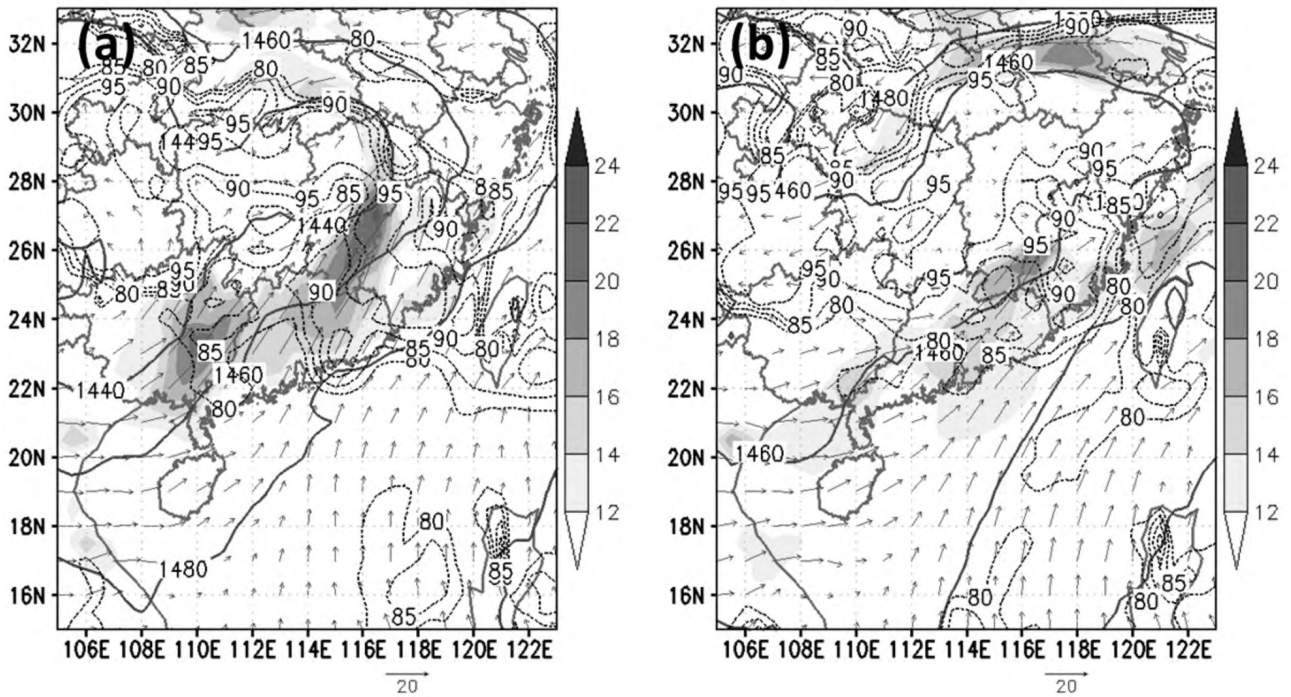

Figure 2. The horizontal wind speed (greater than 12 m s^{-1}, shaded, unit: m s^{-1}), wind vectors (gray arrows), geopotential height (thick solid lines, contour interval of 20 gpm) and relative humidity (greater than 80%, thin dashed lines, contour interval of 5%) at 850 hPa at 0000 UTC 15 (a) and 0000 UTC 16 (b) May 2013.

low vortex stayed at the South China region and moved into Guangdong constantly. The low-level jet played an important role in the formation and development of this heavy rainfall. On the one hand, moisture was transported from the Bay of Bengal and the South China Sea to South China by the low-level jet, increasing the humidity and unstable energy there; On the other hand, there was dynamical convergence at the left front of the low-level jet, which was in favor of air lifting.

2.2 *Experiment design*

With the objective of studying the impact of different physical processes and their parameterizations on the performance of short-range precipitation prediction for AFRS, an EPS using multi-physics was established and used to implement corresponding experiments.

The numerical model we used is the GRAPES mesoscale model, which employs the semi-implicit semi-Lagrangian scheme for integration of time and terrain-following coordinate in the vertical direction. The domain of model covers the range of 96° to 130.6° E, 11° to 38.4° N, with horizontal resolution of 0.09° in both longitude and latitude, and has 385×305 horizontal grid points. There are 55 layers in the vertical direction and the model top is at the height of 35 000 m. Rapid Radiative Transfer Model (RRTM) longwave and Dudhia's shortwave radiation scheme are used, while Monin-Obukhov scheme is employed for surface layer physics.

On the short-range precipitation prediction with numerical models, four sets of physical processes parameterizations, namely, cumulus (hereafter, CU), microphysics (hereafter, MP), land surface (hereafter, LS) and PBL have the most significant influence. Therefore, this study used these four sets of parameterization to construct a multi-physics EPS. That was, the EPS was run with combinations of these different sets of parameterization with different schemes. The rationale of the schemes used in this study will be described briefly in the following sections.

CU is intended to model the sub-grid-scale motion (i.e., updrafts and downdrafts) in the atmosphere related to cumulus convection. When the NWP model is run in the horizontal resolution range of 4 to 10 km, convection is partially resolved and partially unresolved. In this situation, use of CU may violate the underlying assumptions and closure hypotheses on which CU is based (Arakawa and Chen [22]; Molinari and Dudek [23]; Hammarstrand [24]). For example, in classical mass flux schemes, net mass transport is assumed not to exist in the convective grid column. However, this assumption is not valid for NWP models run in the horizontal resolution of a few kilometers (Yu and Lee [25]). In addition, mesoscale models, with horizontal resolution of around 10 km, cannot entirely represent convective clouds explicitly. These models form updrafts and downdrafts on a scale much larger than that in nature (Kuell et al.[26]). In recent works, use of CU in NWP models in such resolutions is proved to be able to improve the performance of NWP (Yu and Lee [25]; Deng and Stauffer[27]; Kotroni and Lagouvardos [28]; Niemelä and Fortelius[29]). Nevertheless, there is no decisive conclusion on whether CU should be used for such resolution or not [25, 27].

Therefore, this study also used a cumulus-free option as an alternative scheme (hereafter, NONE) for cumulus parameterization. The other schemes for CU used in this study were simplified Arakawa-Schubert (SAS) (Arakawa and Schubert[30]; Grell[31]; Pan and Wu[32]; Han and Pan[33]), Betts-Miller-Janjic (B-M-J) (Betts[34]; Betts and Miller[35]; Janjic[36-37]); and Kain-Fritsch (K-F) (Kain and Fritsch [38-39]). The SAS scheme uses a simple concept model, in which air in cloud is composed of an updraft and a downdraft. Moreover, only the spectrum of cloud for the deepest convection is used to model the interactions between the cumulus cells and large-scale environment. As a convective-adjustment scheme, the B-M-J scheme adjusts the lapse rates of temperature and moisture to the quasi-equilibrium reference thermodynamic lapse rate, during the process of large-scale convergence and convection. The impacts of deep and shallow convection are both taken into account, treated with different reference thermodynamic lapse rates. Based on a simple cloud model with moist updrafts and downdrafts, the K-F scheme includes the effects of detrainment and entrainment, as well as relatively simple microphysics.

MP is employed to model the processes resulting in different forms of precipitation, such as rain, snow and hail. The schemes for MP used in this study were WRF single moment 6-class (WSM6) (Lin et al.[40]; Hong and Lim [41]; Dudhia [42]), NCEP 3-class (hereafter, NCEP3) (Hong et al.[43-44]) and CMA simple mixed phase explicit cloud (hereafter, Simple) (Hu et al.[45]; Liu et al.[46]). The WSM6 scheme includes six classes of hydrometeors: water vapor, rain, snow, cloud water, cloud ice and graupel. The NCEP3 scheme predicts only three categories of hydrometers: water vapor, cloud water (cloud ice) and rain (snow), assuming cloud water (ice) and rain (snow) for temperature above (below) freezing. The Simple scheme also predicts three categories of hydrometers. One of them is water vapor, and the others are determined according to the temperature. Specifically, they are cloud water (super-cooled water) and rain (snow) in warm (cold) regions with temperature above (below) freezing.

LS is utilized to describe surface heat and moisture fluxes. The schemes for LS used in this study are 5-layer thermal diffusion (SLAB) (Blackadar[47-48]; Dudhia[49]) and 4-layer Noah LSM (hereafter, NOAH) (Chen and Dudhia [50]; Ek et al.[51]). The SLAB scheme divides soil into five layers. Each layer includes both the upward and downward heat fluxes and the corresponding temperature is predicted through the thermal equilibrium equation. The NOAH scheme consists of one canopy layer with water stored on it, and a 4-layer soil temperature and moisture model. It predicts not only soil temperature, but also soil moisture and runoff.

PBL is used to model the vertical sub-grid-scale fluxes due to eddy transport. The schemes for PBL adopted in this study were Medium Range Forecast Model (MRF) (Hong and Pan[52]) and Yonsei University (YSU) (Hong et al.[53]; Hong[54]). The MRF scheme calculates the counter-gradient flux for heat and moisture in unstable conditions, and uses enhanced vertical flux coefficients. The YSU scheme adds explicit treatment of the entrainment layer at the PBL top to the MRF scheme and reduces the magnitude of counter-gradient terms to make the stratification of PBL more neutral.

The four schemes for CU, the three schemes for MP, the two schemes for LS and the two schemes for PBL mentioned above were combined, resulting in 48 ($4\times3\times2\times2$) members in EPS. However, some of these 48 members cannot do the integration stably. As a result, the 14 members with unstable integration were eliminated and the remaining 34 members were used to construct EPS. For every member in EPS, the initial condition was from GFS analysis data with $0.5^{\circ}\times0.5^{\circ}$ horizontal resolution, while the lateral boundary conditions were from GFS forecast data with $0.5^{\circ}\times0.5^{\circ}$ horizontal resolution at a frequency of 6 hours. EPS was initialized at 1200 UTC 14 May 2013 for issue of 36-h forecasts.

3 RESULTS OF EXPERIMENTS

This study is focused on short-range prediction of AFRS, especially the heavy rainfall in Guangdong province. Therefore, we mainly discuss the forecasting results of EPS at the Guangdong area (108°–119°E, 18°-26°N, hereafter, GD) in the remaining part of the article.

3.1 *Experiment design*

The 24-h accumulated predicted rainfall of different ensemble members from 0000 UTC 15 May to 0000 UTC 16 May is shown in Fig.3. In Fig.3, numbers in black, red, blue and purple represent the schemes for MP (1 indicates WSM6, 2 indicates NCEP3, 3 indicates Simple), PBL (1 indicates MRF, 2 indicates YSU), LS (1 indicates SLAB, 2 indicates NOAH) and CU (0 indicates NONE, 1 indicates SAS, 2 indicates B-M-J, 3 indicates K-F), respectively. When the SAS scheme is used for CU, for the given scheme for LS, the corresponding pattern of precipitation is nearly the same, no matter the MRF or YSU scheme is adopted for PBL. For example, there is little difference among 1111, 2111, 3111, 1211 and 2211 in Fig.3. Similarly, changing the scheme for MP dose not induce obvious variation of precipitation pattern. For instance, 1121, 2121 and 3121 in Fig.3 are similar between each other. In sharp contrast, there are marked differences of precipitation pattern among members using different schemes for LS. For example, 1111 differs from 1121 prominently. When the B-M-J, K-F, or NONE scheme is used for CU, findings mentioned above are also prominent. Thus it can be seen that, for a given scheme for CU, the precipitation pattern is most sensitive to the change of LS scheme.

When the scheme for LS is specific, changing the

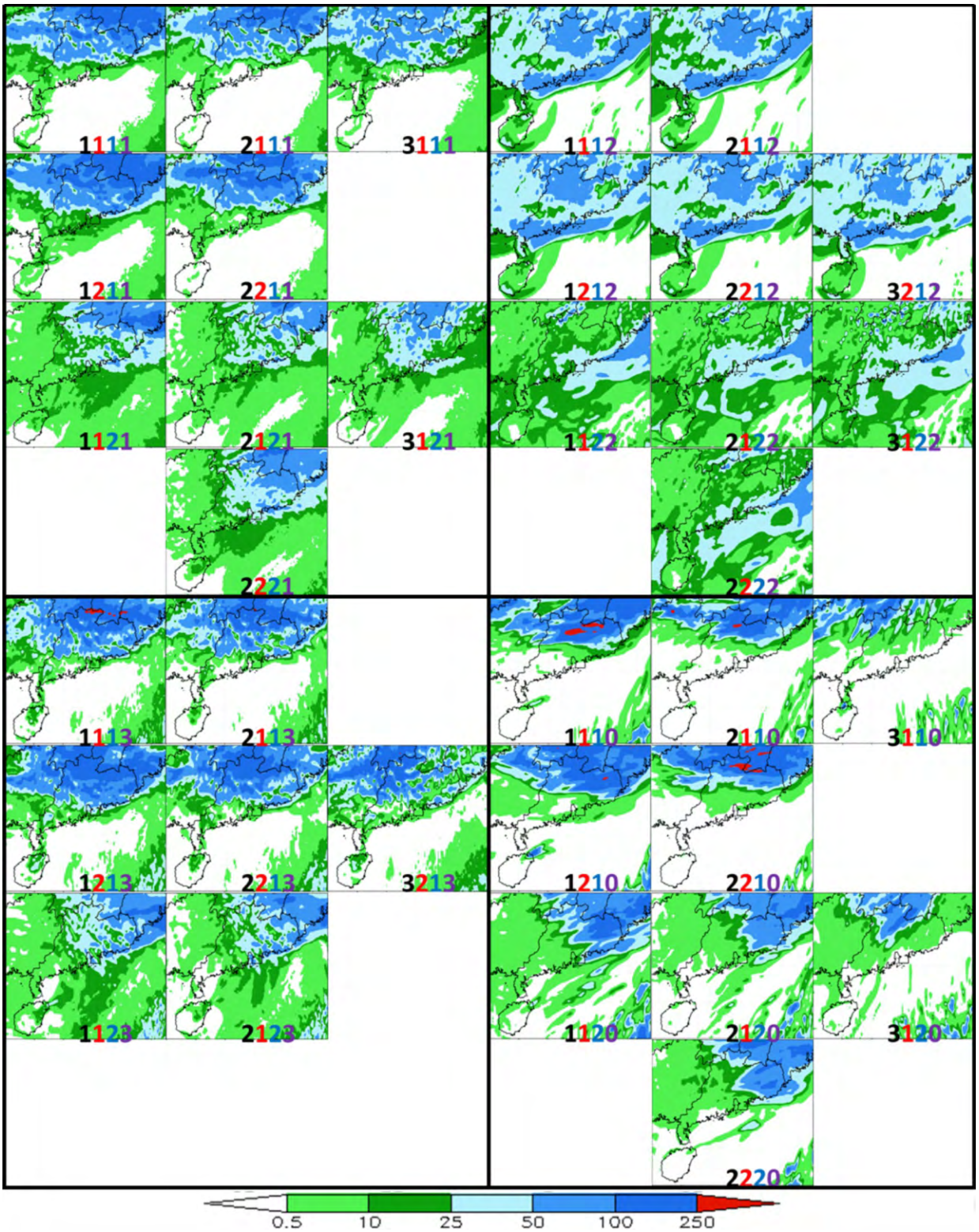

Figure 3. 24-h accumulated predicted rainfall (unit: mm) of different ensemble members from 0000 UTC 15 May to 0000 UTC 16 May 2013.

scheme for CU results in large differences of precipitation pattern. In particular, differences of precipitation pattern between members with SAS and those with K-F are small, while differences between members with B-M-J and those with SAS or K-F are large. For instance, 1111 extremely resembles 1113, and both of them are very different from 1112. Additionally, turning CU off causes evident change of precipitation pattern.

As the scheme for CU and that for LS are both specific, changing the scheme for MP leads to a slight

difference of precipitation pattern. Particularly, there are small differences of precipitation pattern between members with WSM6 and those with NCEP3, while there are large differences between members with Simple and those with WSM6 or NCEP3. For example, both 1110 and 2110 are very different from 3110.

The analysis above shows that, prediction of precipitation pattern is most sensitive to the change of CU and LS scheme, followed by the change of MP scheme, while changing PBL scheme results in the least influence on it. Besides, the members (e.g. 2211) with the SAS (or K-F) scheme, coupled with the WSM6 (or NCEP3), SLAB and YSU schemes, predict the precipitation pattern closest to the observations. On the contrary, the members (e.g. 3122) with the B-M-J (or NONE) scheme, coupled with the Simple, NOAH and MRF schemes, predict the precipitation pattern furthest from the observations.

The 24-h accumulated predicted rainfall for the threshold of 0, 50 and 200 mm of different ensemble members is averaged over GD (Fig.4a, c, e), respectively. Correspondingly, the numbers of grids for these thresholds are divided by the numbers of grids for the whole GD domain (Fig.4b, d, f), respectively, to calculate the "ratio" to represent the area of precipitation (hereafter, area ratio).

In the four physical processes, changing LS scheme causes the largest variation of both magnitude and area of precipitation, no matter for the light rainfall (> 0 mm) or the heavy rainfall (> 50 mm and > 200 mm). For the light rainfall, choosing the SAS, WSM6, MRF and SLAB scheme for CU, MP, PBL and LS, respectively predicts precipitation amount of 42.92 mm and area ratio of 0.64. If the LS scheme is changed from SLAB to NOAH, the predicted precipitation amount and area ratio change to 18.91 mm and 0.95, with variation of 24.01 mm and 0.31, respectively. If the CU scheme is changed from SAS to B-M-J, the predicted precipitation amount and area ratio change to 36.45 mm and 0.69, with variation of 6.47 mm and 0.05, respectively. If the MP scheme is changed from WSM6 to NCEP3, the predicted precipitation amount and area ratio change to 36.62 mm and 0.58, with variation of 6.3 mm and 0.06, respectively. If the PBL scheme is changed from MRF to YSU, the predicted precipitation amount and area ratio change to 45.65 mm and 0.73, with variation of 2.73 mm and 0.09, respectively. For the rainstorm (> 50 mm), the variation of precipitation magnitude and area, resulted from changing CU scheme, is second only to that resulting from changing LS scheme. For example, the largest variation of precipitation amount resulting from changing CU scheme reaches up to 52.35 mm. For the torrential rain (>200 mm), changing MP scheme causes prominent variation of precipitation magnitude and area, only smaller than that caused by changing LS scheme. For example, the largest variation of precipitation amount caused by changing MP scheme reaches up to 253.36 mm. Therefore, it is suggested that LS has the greatest impact on prediction of precipitation magnitude and area for this case, while the impacts of CU and MP are mainly concentrated in heavy rainfall. Although problems are dealt with more comprehensively in NOAH than in SLAB, there are still some drawbacks in NOAH, especially in the calculation of net radiation and liquid water content. As a consequence, ground heat and moisture fluxes of the members with the NOAH scheme differ much from those of members with the SLAB scheme, resulting in large differences in the corresponding prediction of precipitation magnitude and area.

The precipitation magnitude of members with the SAS scheme is close to that of members with the K-F scheme and larger than that of members with the B-M-J scheme. For the light rainfall (Fig.4b) and rainstorm (Fig.4d), members with the SAS scheme and those with the K-F scheme behave quite similarly in terms of precipitation area; whereas, for torrential rain, the precipitation area of the latter is larger compared with the former (Fig.4f). In the members with cumulus option on, those with the B-M-J scheme predict the smallest area for the heavy rainfall (Fig.4d, f). Moreover, turning cumulus option off leads to increment of precipitation magnitude. Considering precipitation area of the light (heavy) rainfall, it decreases (increases) after turning cumulus option off. It is thus clear that, use of CU tends to produce light rainfall with large area, but not in favor of generating local heavy rainfall. Compared to the NOAH scheme, use of the SLAB scheme for LS gives rise to larger precipitation magnitude (Fig.4a, c, e), no matter for the light rainfall or heavy rainfall. For area of the light (heavy) rainfall, the members with the SLAB scheme produce larger (smaller) one than those with the NOAH scheme (Fig.4b, d, f). Therefore, it can be concluded that, the NOAH scheme avails the generation of large-area light rainfall, while the SLAB scheme is good for producing heavy rainfall in isolated area. For the two schemes for PBL, namely MRF and YSU, there is little difference of precipitation magnitude and area between them. Among the three schemes for MP, the Simple scheme produces the smallest precipitation magnitude and area. Besides, there are larger precipitation magnitude and area for members with the WSM6 scheme than for those with the NCEP3 scheme. That is to say, the former produces local heavy rainfall more easily than the latter.

3.2 *Characteristics of synoptic pattern*

The 1-h accumulated predicted rainfall for threshold of 2 mm (Fig.5a), horizontal wind speed greater than 12 m s^{-1} (i.e. low-level jet, Fig.5c), relative humidity greater than 80% (Fig.5d) and divergence less than 0 (Fig.5e) at 850 hPa in GD of members with the SAS scheme are averaged over the corresponding grids. The vertical integrated convective available potential energy (CAPE) is averaged over GD (Fig.5b), and the numbers

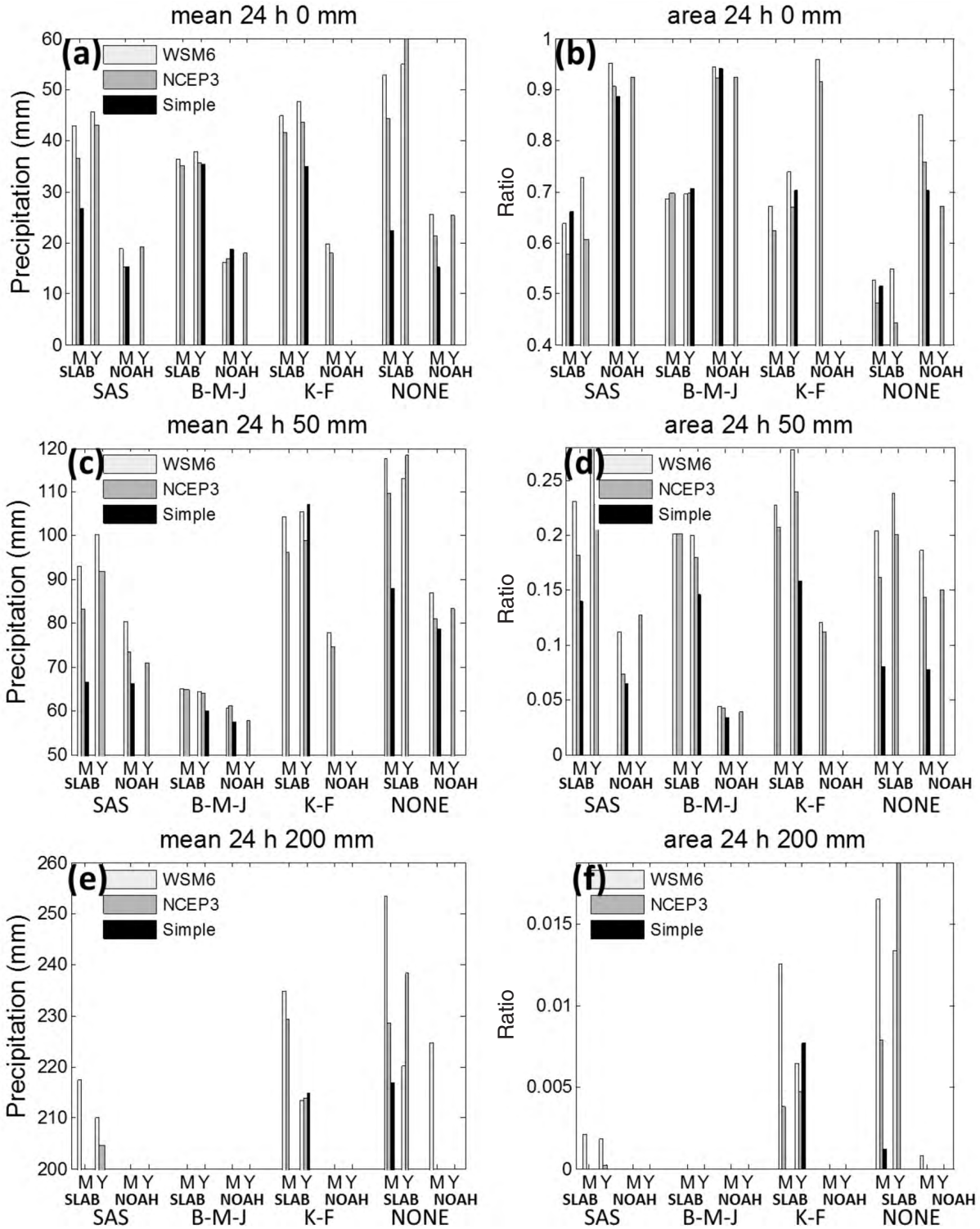

Figure 4. Mean (left column) and area ratio (right column) of 24-h accumulated predicted rainfall in the GD domain for threshold of 0 (a, b), 50 (c, d), 200 (e, f) mm for different ensemble members from 0000 UTC 15 May to 0000 UTC 16 May 2013. For the abscissas, (a) and (b) correspond to PBL (M represents MRF, Y represents YSU), (c) and (d) correspond to LS, and (e) and (f) correspond to CU. Shaded legend corresponds to MP.

of grids for relative humidity greater than 80% in GD are divided by the numbers of grids for the whole GD domain to calculate the corresponding area ratio (Fig. 5f). In Fig.5, lines in black and green indicate the SLAB and NOAH scheme for LS, respectively; lines in mauve and cyan indicate the YSU and MRF scheme for PBL, respectively; markers in mauve and cyan indicate the YSU and MRF scheme for PBL, respectively; circle (○), square (□), diamond (◇) indicate the WSM6, NCEP3 and Simple scheme, respectively. We can see

from Fig.5a that, different physical processes have different impacts on the characteristics of synoptic pattern. There are obvious differences of thermodynamics variables, such as CAPE (Fig.5b) and relative humidity (Fig.5d, f), as well as dynamics variables, such as low-level jet (Fig.5c) and wind convergence at lower levels (Fig.5e), between members with different LS scheme. For MP, the obvious differences resulting from changing scheme are mainly concentrated on dynamics variables. For the amount of heavy rainfall, changing MP scheme causes the most prominent variations, compared with changes of scheme for the other three physical processes (Fig.5a).

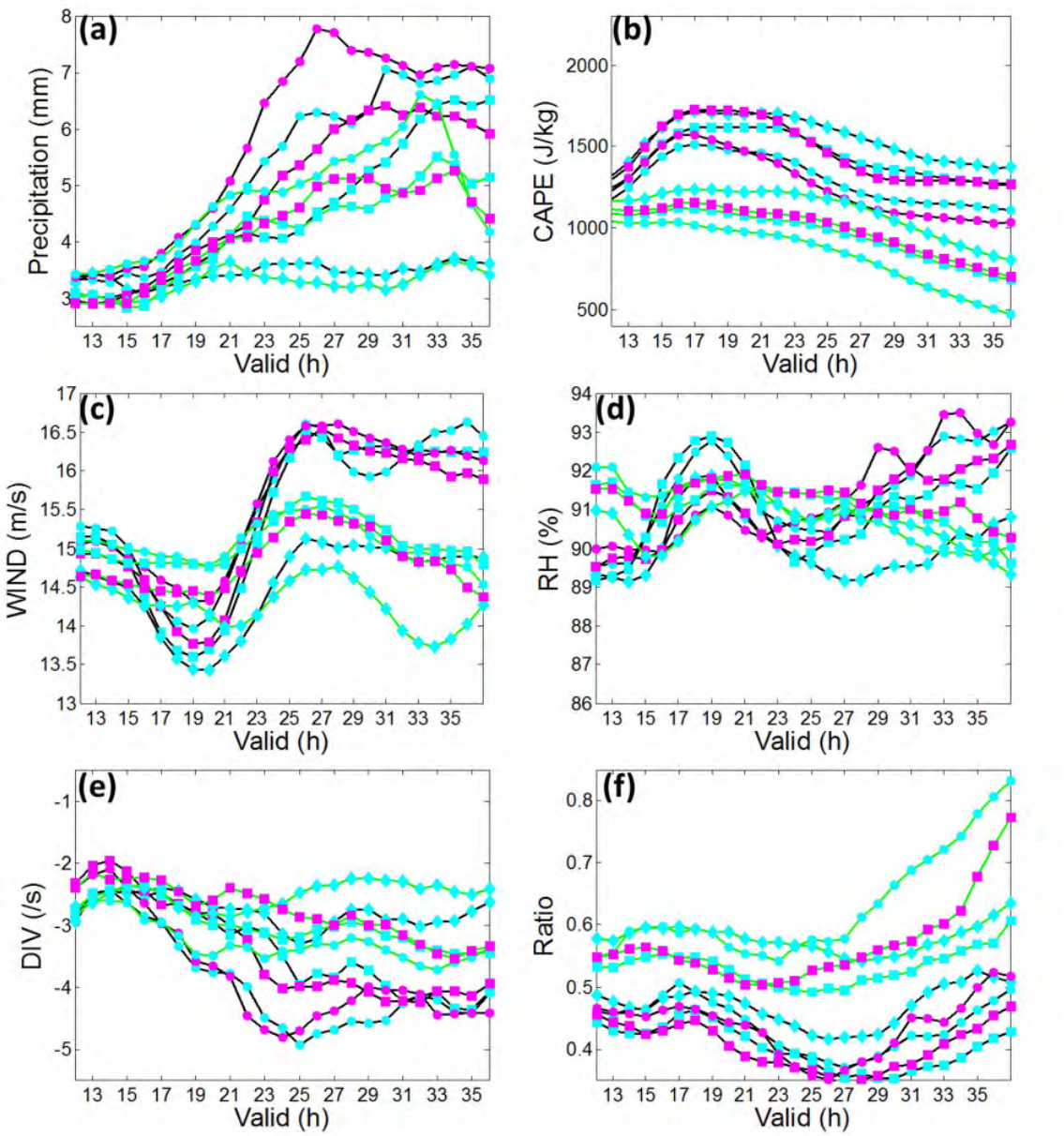

Figure 5. Time evolution for mean of 1-h accumulated predicted rainfall greater than 2 mm (a), mean of convective available potential energy (b), mean of horizontal wind speed greater than 12 m s^{-1} at 850 hPa (c), mean of divergence less than 0 s^{-1} at 850 hPa (e), mean (d) and area ratio (f) of relative humidity greater than 80% at 850 hPa in the GD domain for ensemble members with CU using SAS.

There are some correlations in time between the intensification of low-level jet and the enhancement of wind convergence at lower levels for this case, especially after the 18-h forecast time (Fig.5c, e), as the SAS scheme used for CU. Using the Simple scheme leads to the smallest precipitation amount in Fig.5a, with most obvious discrepancy after the 18-h forecast time (Fig.5a). This result may be related to the weaker low-level jet (Fig.5c) and wind convergence at lower levels (Fig.5e) after this time, compared with other members. With the WSM6 scheme, the predicted precipitation amount is larger than that with the NCEP3 scheme. The stronger low-level jet (Fig.5c) and higher (Fig.5d) and broader (Fig.5f) humidity concentration

predicted with the WSM6 scheme may be responsible for the corresponding larger precipitation amount. The members using the SLAB scheme for LS predict greater precipitation amount than those using the NOAH scheme (Fig.5a). On the one hand, in the former, CAPE with larger strength (Fig.5b) and area maintains for the whole forecasts, and a stronger low-level jet (Fig.5c) maintains from the 21-h forecast time to the end. On the other hand, there is higher humidity concentration in the former, especially in the last 9 hours of forecast (Fig.5d). For the latter, the predicted area of humidity concentration is larger (Fig.5f), leading to more large-area light rainfall. For PBL, use of the YSU scheme causes larger precipitation amount, especially after the 21-h forecast time, compared to the MRF scheme (Fig.5a). In the former, the low-level jet is stronger after the 15-h forecast time and humidity concentration is higher after the 21-h forecast time, causing heavier rainfall. From the discussion above, we can find that the greatest impact on the precipitation amount for this heavy rainfall event comes from the low-level jet. All the members with larger precipitation magnitude predict a stronger low-level jet, especially in the last 12 hours of forecast. Also, the members with the most marked intensification of the low-level jet predict the most enhancement of precipitation magnitude (Fig.5a, c). The local humidity concentration also has certain impact on the precipitation magnitude. Specifically, higher and broader humidity concentration coincides with heavier rainfall. Compared with the other schemes, the WSM6/SLAB/YSU scheme for MP/LS/PBL produces a stronger low-level jet and higher humidity concentration. The impact of CAPE on the precipitation magnitude is smaller, compared to the other factors discussed above. Among different schemes for the same physical process, the Simple/SLAB/MRF scheme for MP/LS/PBL produces stronger CAPE than the other schemes.

To explore the impact of different physical processes and their parameterizations on the prediction of thermodynamics processes, the apparent heat source Q_1 and the apparent moisture sink Q_2 predicted by EPS are calculated and averaged over GD to get the vertical profiles (Fig.6, the schemes indicated by different colors or markers are the same as those in Fig.5).

The apparent source Q_1 and the apparent moisture sink Q_2 in the p-coordinate are calculated from

$$Q_1 = Q_R + L(c-e) - \frac{\partial}{\partial p}\overline{s'\omega'} \quad (1)$$

$$Q_2 = L(c-e) + L\frac{\partial}{\partial p}\overline{q'\omega'} \quad (2)$$

where Q_R is the radiative heating rate, L the latent heat of condensation, c the rate of condensation, e the rate of evaporation of cloud water, s the dry static energy, ω the vertical p-velocity, and q the mixing ratio of water vapor. "—" denotes the average of variables while "□" denotes the deviation from the average. Q_1 is composed of the radiative cooling, latent heating and sub-grid scale vertical transport of heat, while Q_2 is composed of the latent heating and sub-grid scale vertical transport of moisture. The physical processes associated with the vertical transport include cumulus convection and eddy. In the heavy rainfall, Q_R is generally smaller than the other terms in Eq. (1) to be neglected (Kuo et al. [55]). From Eq. (1) and Eq. (2) we can learn that, cumulus convection can generate feedback on large-scale environment by release of latent heat and vertical transport of heat and moisture. As a result, the characteristics of vertical distribution of Q_1 and Q_2 can be utilized to learn the features of heating processes and precipitation. If the vertical profiles Q_1 of Q_2 are very similar, the convection is weak and heating is mainly due to the condensation related to stratiform clouds; if the vertical profiles of Q_1 and Q_2 differ from each other and there is a separation in the levels of peak values of Q_1 and Q_2, the vertical transport of heat and moisture by convection is strong, as well as the release of latent heat is related to cumulus convection (Yanai et al. [56]; Thompson [57]). The difference of Q_1 and Q_2 serve to measure the intensity of cumulus convection, namely larger difference standing for larger intensity (Yanai et al.[56]; Yanai and Johnson[58]).

At the 18-h forecast time (i.e. 0600 UTC 15 May), the vertical profiles of apparent heat source corresponding to the SLAB and NOAH scheme differ from each other very much, with more intense heating at higher (lower) levels for the former (latter) (Fig.6a). At this time, there are no obvious peak values of apparent heat source in the vertical, whereas apparent moisture sink has a peak at the height of 700 to 600 hPa. This phenomenon shows that the predicted heating in the troposphere is due to the release of latent heat in deep cumulus convection. Compared with the NOAH scheme, the SLAB scheme is found to have a larger peak for the predicted apparent moisture sink, indicating more convective precipitation. There is a large negative value of apparent moisture sink corresponding to the NOAH scheme at lower levels, showing large accumulation of moisture there which coincides with broad humidity concentration (Fig.5f). Apparent heat source for all the members increases at the middle and higher levels with model integration, with two peak values in the vertical at 100 hPa and 400 to 500 hPa respectively (Fig.6c, e). The increment of apparent moisture sink with model integration is more significant than that of apparent heat source (Fig.6d, f), reflecting the increment of convective precipitation. Just because of this, the differences between apparent heat source and apparent moisture sink also improve with time, as an indication of improvement for vertical transport of heat and moisture. Comparing the SLAB, YSU and WSM6 scheme with the NOAH, MRF and NCEP3 (or

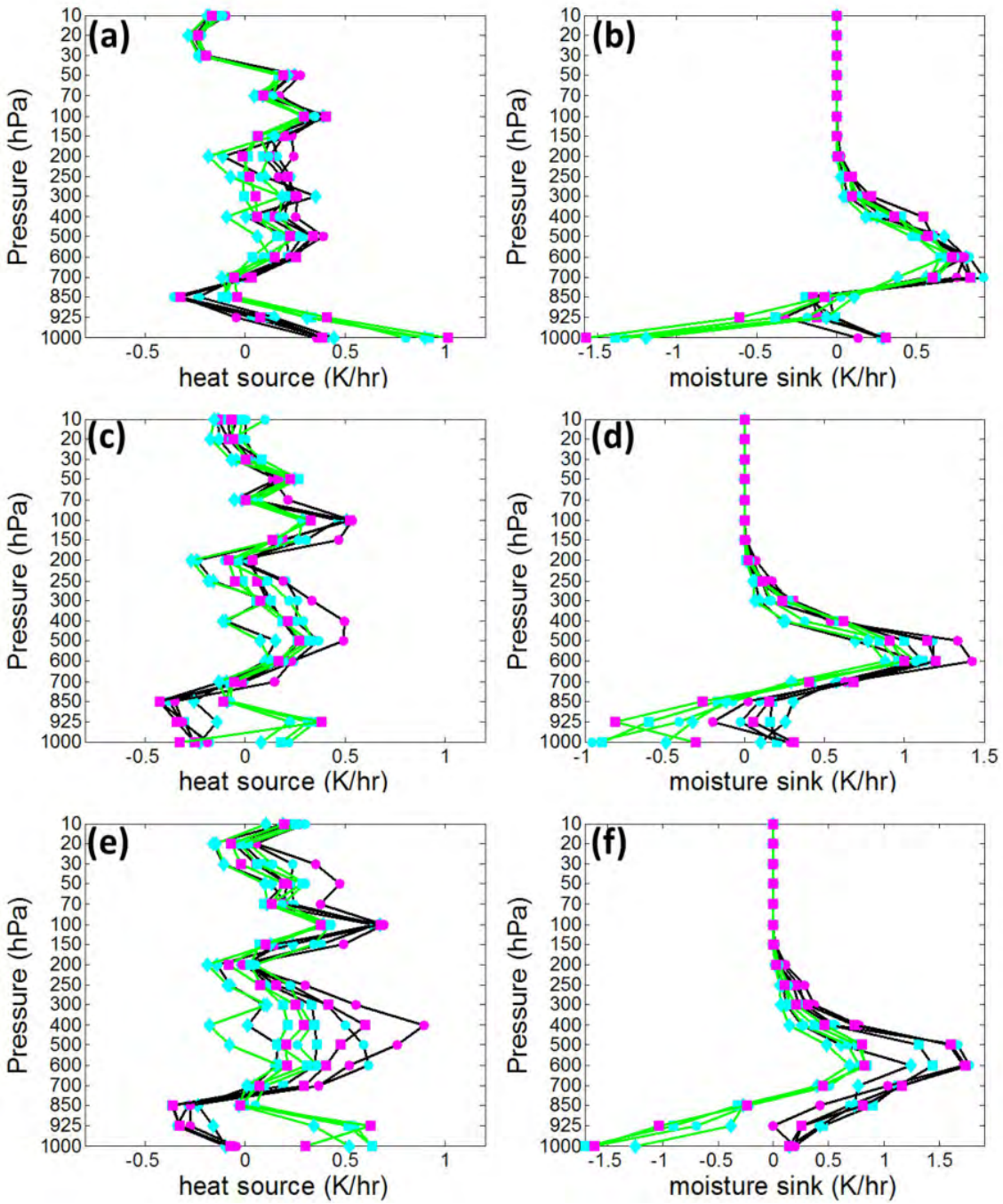

Figure 6. Vertical profile of apparent heat source (left column) and apparent moisture sink (right column) in the GD domain for ensemble members with CU using SAS at 0600 UTC 15 (a, b), 1200 UTC 15 (c, d) and 1800 UTC 15 (e, f) May 2013.

Simple) scheme, respectively, we can see that the former group gives more remarkable increments of apparent moisture sink with time as well as larger precipitation magnitude. Apparent moisture sink gets the most prominent enhancement during the 18-h to 30-h forecast time, so do the precipitation magnitude (Fig. 5a), low-level jet (Fig.5c) and wind convergence at lower levels (Fig.5e). That is to say, there are some positive correlations among the low-level jet, wind convergence at lower levels, precipitation and release of latent heat.

The results for comparison of precipitation magnitude, CAPE, low-level jet, wind convergence and humidity at lower levels, as well as apparent heat source and apparent moisture sink, among different members with the K-F scheme, is somewhat similar to those in the case of the SAS scheme (not shown), so we do not discuss them here.

As discussed earlier, choosing the B-M-J scheme for CU leads to smaller precipitation magnitude and area for heavy rainfall, as compared with those given by the other CU schemes; by contrast, turning cumulus

option off leads to increment of them. Hence, we compare CAPE, low-level jet, wind convergence and humidity at lower levels predicted using the B-M-J scheme and without CU (left and right columns in Fig. 7, the schemes indicated by different colors or markers are the same as those in Fig.5) with those using the SAS scheme (Fig.5), respectively. CAPE given by the B-M-J scheme is below 1 400 J kg^{-1}, smaller than that given by the SAS scheme (Fig.7a); whereas, no-cumulus members give larger CAPE, especially with the SLAB or Simple scheme (Fig.7b). The low-level jet predicted by members with the B-M-J scheme is weaker, coupled with the NOAH scheme in particular (Fig.7c), and so does the corresponding wind convergence at lower levels (Fig.7f). Turning cumulus option off results in certain impacts on the evolution of the low-level jet. In detail, its intensification is more intense during the 6-h to 12-h forecast time (not shown); the reduction is more gentle during the 12-h to 18-h forecast time. In the last 12-h forecast, the intensity of low-level jet without CU is between that with the SAS and B-M-J scheme (Fig. 7d). At the same time, wind convergence at lower levels also exhibits intensification (Fig.7f). The humidity concentration is much lower, with magnitude below 91% (Fig.7g), but very broader (Fig.7i). With CU turned off, humidity concentration is slightly higher (Fig.7h) and broader (Fig.7j). These results suggest that, lighter precipitation with the B-M-J scheme is mainly due to the weaker low-level jet and lower humidity concentration; while stronger wind convergence at lower levels and higher humidity concentration in no-cumulus members contribute to their heavier precipitation.

Figure 8 shows the vertical profiles of apparent heat source and apparent moisture sink for ensemble members with CU using B-M-J and without CU, in which the schemes indicated by different colors or markers are the same as those in Fig.5. In the first 18-h forecast, the vertical profiles of apparent heat source and apparent moisture sink with and without CU are similar (not shown). At the 24-h forecast time, apparent heat sources for members with the B-M-J scheme are similar to each other, with small values near 9 K h^{-1} (Fig.8a). Furthermore, the peak value at lower levels lies near 300 hPa, higher than that with the SAS scheme (Fig.6c). The difference between apparent heat source and apparent moisture sink is smaller with the B-M-J scheme than that with the SAS scheme (Fig.8b), and this conclusion also can be seen in the following forecasts (not shown). Turning CU off increases the difference of apparent heat source between the members. In this situation, noticeable cooling occurs at the middle and higher levels for members with the Simple scheme. However, the other members exhibit larger heating compared with those with CU turned on (Fig.8c). Meanwhile, both apparent heat source and apparent moisture sink have a peak value at 500 to 600 hPa, which indicates that stratiform rain dominates the precipitation process. It also can be found that, turning CU off causes apparent moisture sink to enhance evidently and increases the difference between it and apparent heat source slightly (Fig.8d), which may be due to the improvement of vertical transport of heat and moisture by eddy under this condition. To sum up, there is lower proportion and smaller intensity of convective rain given by the B-M-J scheme, when compared with that given by the SAS or K-F scheme; turning CU off improves the proportion of stratiform rain and the impact of eddy vertical transport in PBL on precipitation.

Besides, there are some results similar to those discussed above with the SAS scheme. Under the circumstance of using the B-M-J scheme or turning CU off, changing LS leads to evident variation in both thermodynamics and dynamics variables, while variation caused by changing MP is focused mainly on dynamics variables and heavy rainfall.

In the comparison of members with different CU schemes, we can see that changing CU scheme results in significant variation in thermodynamics and dynamics variables, as well as heavy rainfall.

3.3 *Discussion*

The discussion above showed that, different members differ in the prediction for pattern, magnitude and area of precipitation, as well as wind, temperature and humidity of synoptic pattern in this event of AFRS. When the NCEP3, YSU, SLAB and SAS scheme are chosen for MP, PBL, LS and CU respectively (i.e. 2211), the predicted precipitation is much closer to observation, compared to all the other combinations. In contrast, the members with the Simple scheme, coupled with the MRF, NOAH and B-M-J (or NONE) scheme (i.e. 3122 or 3120), predict the precipitation much further from the observations, compared with all the other members. To understand the cause resulting in the differences of precipitation prediction between different members, we do the comparative analysis of synoptic pattern between 2211 with the best prediction and 3122 as well as 3120 with the worse predictions (Fig.9). The spatial distribution of apparent heat source and apparent moisture sink resemble each other (not shown), indicating that release of latent heat for condensation is the major source of heating in precipitation. Therefore, apparent moisture sink is used to represent latent heat for condensation in the following discussion.

In 2211, heavy 6-h accumulated rainfall occurs in the northeastern Guangdong at the 24-h forecast time (i. e. 1200 UTC 15), coinciding with the larger apparent moisture sink (Fig.9a), namely larger release of latent heat for condensation. At this moment, a strong southwest low-level jet is in central and eastern Guangdong, with significant convergence at the front-left side (i.e. from northeastern Guangdong to southern Jiangxi). In the following 6 hours, precipitation

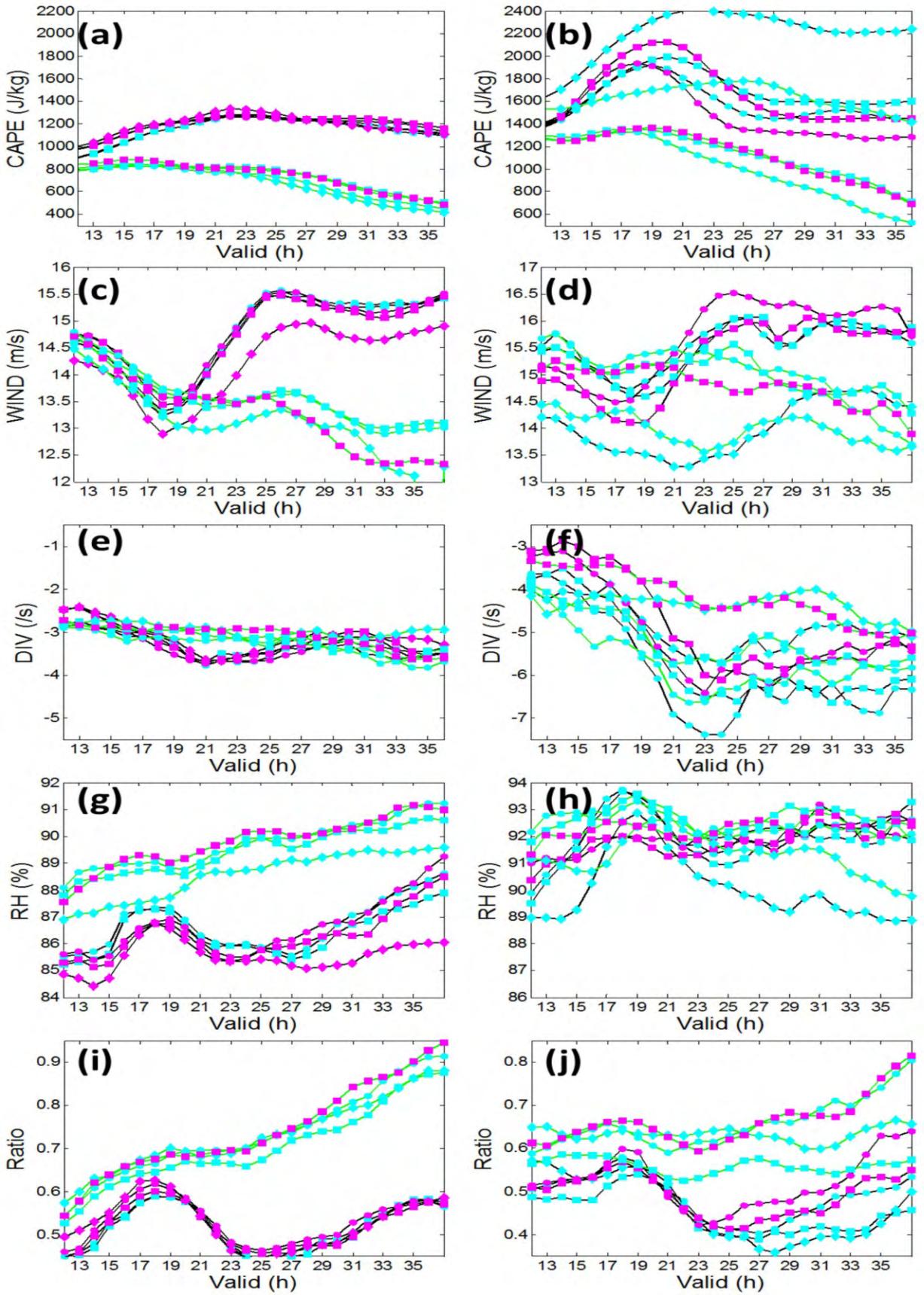

Figure 7. Time evolution for mean of convective available potential energy (a, b), mean of horizontal wind speed greater than 12 m s^{-1} at 850 hPa (c, d), mean of divergence less than 0 s^{-1} at 850 hPa (e, f), mean (g, h) and area ratio (i, j) of relative humidity greater than 80% at 850 hPa in the GD domain for ensemble members with CU using SAS (left column) and NONE (right column).

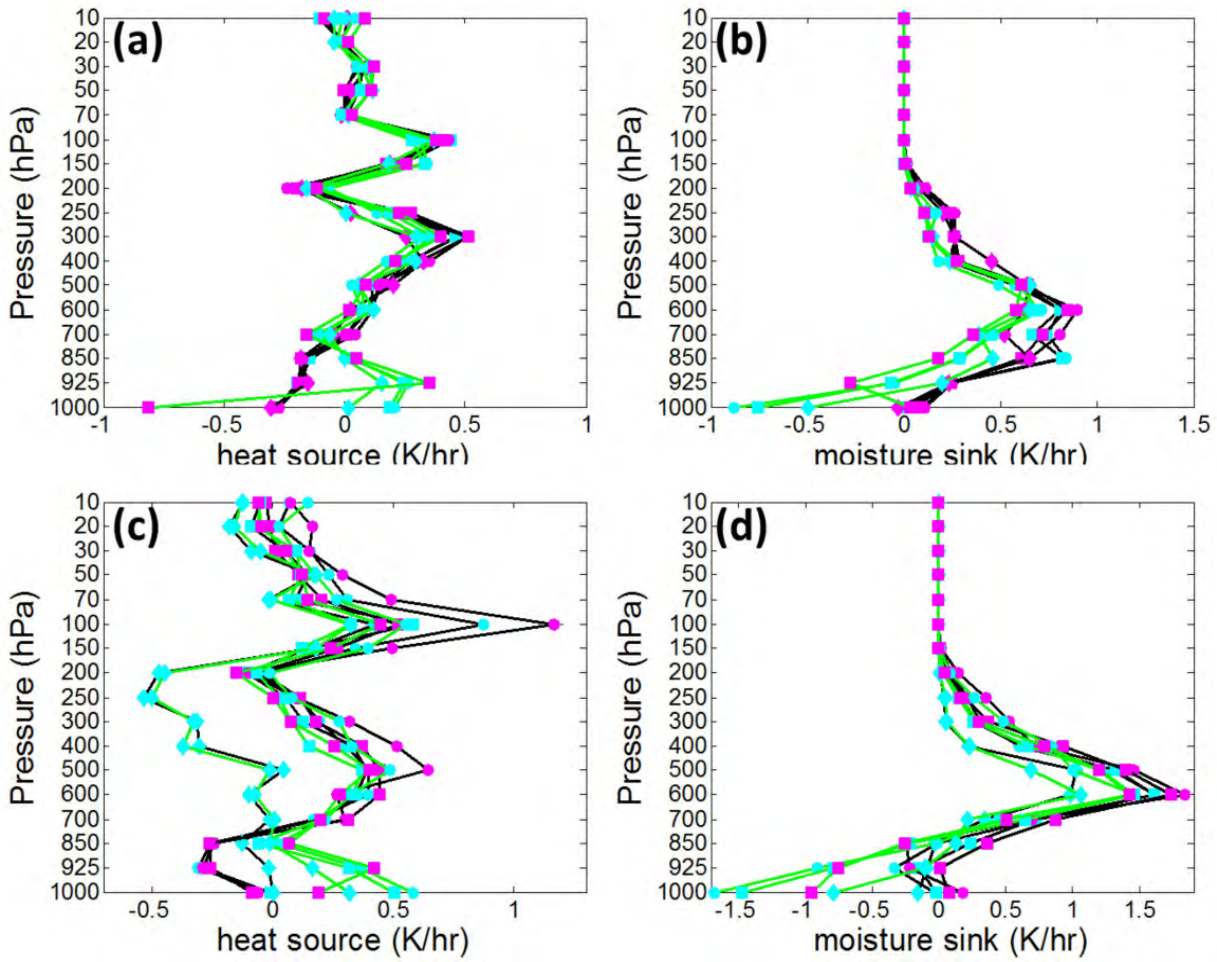

Figure 8. Vertical profile of apparent heat source (left column) and apparent moisture sink (right column) in the GD domain for ensemble members with CU using B-M-J (a, b) and NONE (c, d) at 1200 UTC 15 May 2013.

in the northeastern Guangdong increases constantly and corresponding release of latent heat increases to 30 K h^{-1} (Fig.9b). Strong wind convergence appears in the regions where release of latent heat is large at 1200 UTC 15 May. Besides, a low-level jet, located on the east side of the wind convergence region (i.e. coastal areas in eastern Guangdong and southern Fujian), intensifies noticeably with time (Fig.9b). Therefore, we can see that, there are certain positive-feedback interactions among precipitation, release of latent heat for condensation, wind convergence and low-level jet in this event of AFRS predicted by 2211. Specifically, the intensification of the low-level jet benefits wind convergence at lower levels to strengthen and promote the development of precipitation thereby, while the increment of precipitation enhances the heating in the atmosphere by latent-heat release, favorable for the improvement of wind convergence (divergence) at lower (higher) levels so as to intensify the low-level jet further (Liao and Tan[59]).

The precipitation, release of latent heat for condensation, wind convergence and low-level jet predicted by 3122 are all much weaker than those predicted by 2211, and the corresponding distributions of high values do not match each other well (Fig.9c-d). On the sea, the concentrations of latent-heat release are corresponding with those of wind convergence with large intensity (Fig.9c). However, the precipitation related to these concentrations of wind convergence in the integration is small (Fig.9d). Thus, interactions among precipitation, release of latent heat for condensation, wind convergence and low-level jet are not evident in this event of AFRS predicted by 3122. As a result, wind convergence at lower levels cannot get enough intensification, thereby leading to inaccurate prediction of precipitation pattern and significant underestimation of precipitation magnitude.

Heavy rainfall predicted by 3120 is concentrated in northern Guangdong (Fig.9e-f). At 1200 UTC 15 May, there is a heavy rainfall belt in NE-SW direction at northern Guangdong, consistent with both concentrations of wind convergence and latent-heat release. It can be observed that, these heavy rainfall, wind convergence and latent-heat release are larger than those predicted by 2211 (Fig.9e). With integration, heavy rainfall, wind convergence and latent-heat release

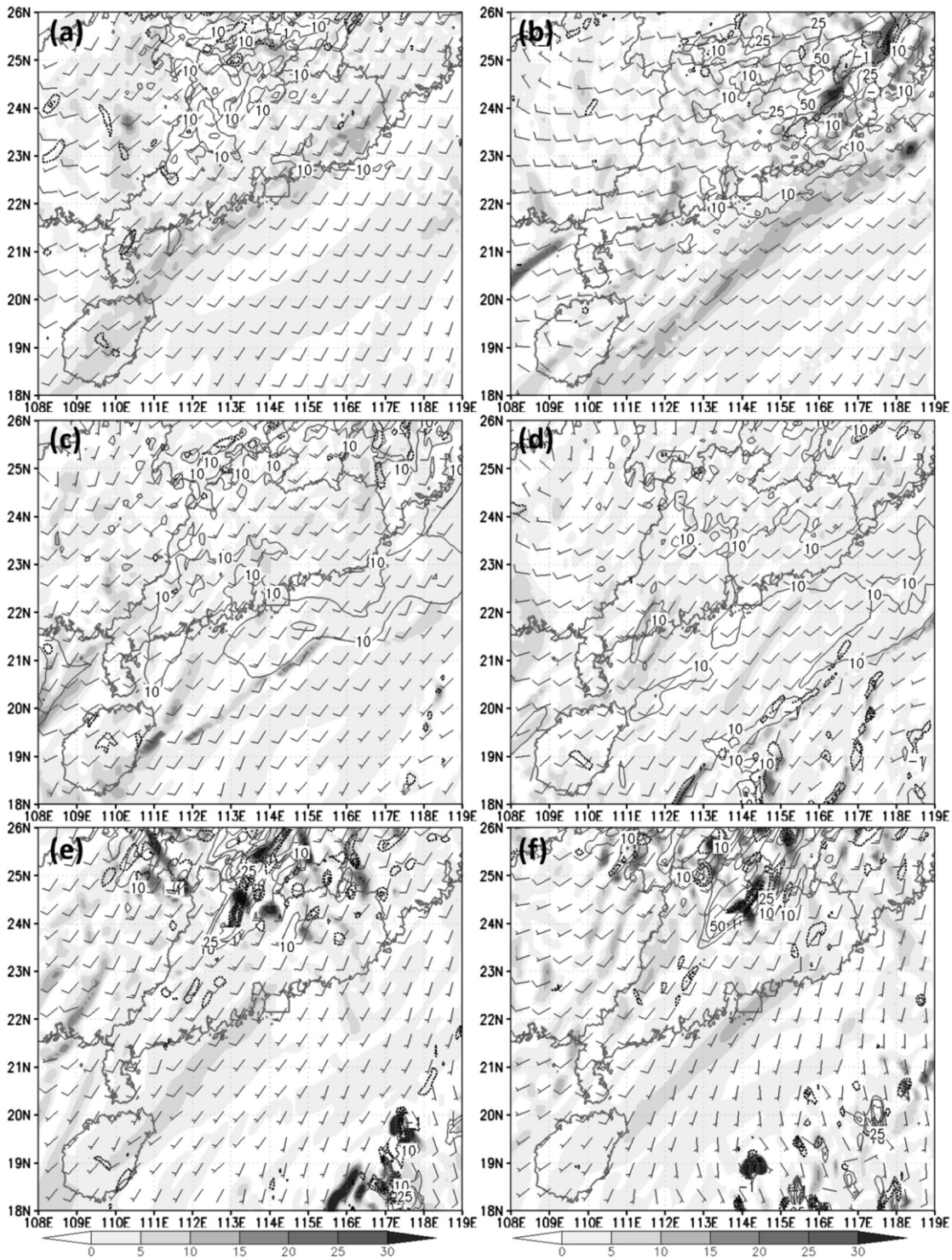

Figure 9. The predicted apparent moisture sink (shaded, unit: K hr-1) at 600 hPa, horizontal wind (barb), negative divergence (dash lines, contour interval of 10^{-4} s^{-1}, unit: 10^{-4} s^{-1}) at 850 hPa and 6-h accumulated rainfall (solid lines, unit: mm) for ensemble members named as 2211 (a, b), 3122 (c, d) and 3120 (e, f) in Fig.3 at 1200 UTC 15 (left column) and 1800 UTC 15 (right column).

all intensify, but the low-level jet remains almost unaltered and is weaker than that predicted by 2211 (Fig.9f). Therefore, interactions among precipitation, release of latent heat for condensation, wind convergence and low-level jet are not depicted well in the prediction of this AFRS event in 3120. Although there are strong wind convergences at lower levels, both the intensity and evolution of low-level jet do not show plausible results. Correspondingly, both the pattern of precipitation and location of heavy rainfall are not predicted accurately, and the magnitude of heavy rainfall is much overestimated.

From the above discussion, conclusions can be drew that, appropriate prediction of interactions among

precipitation, release of latent heat for condensation, wind convergence and low-level jet by numerical models has very important impact on the accurate prediction of the whole precipitation process.

4 CONCLUSIONS

Aiming to understand the impact of different physical processes and their parameterizations on the precipitation prediction of AFRS and improve it thereby, this study employed a multi-physics EPS based on the GRPAES model to perform numerical experiments on an event of AFRS. In the EPS, a set of different schemes for different physical parameterization, namely CU, MP, LS and PBL, was utilized and the members used different combinations of these schemes. From the comparisons of pattern, magnitude and area of precipitation, evolution of synoptic pattern (including low-level jet, wind convergence and humidity at lower levels, CAPE), as well as the vertical distribution of thermodynamics variables (including apparent heat source and apparent moisture sink) among different members, the impact of different physical processes and their parameterizations on the precipitation prediction of this case was discussed.

Selection of schemes for both CU and LS gives the largest impact on the prediction of precipitation pattern, and that of MP and PBL gives the second largest and smallest impact, respectively. Members using the SAS or K-F scheme for CU, coupled with the WSM6 or NCEP3 scheme for MP, the SLAB scheme for LS and the YSU scheme for PBL, exhibit the best performance; while those using the B-M-J scheme for CU or turning CU off, coupled with the Simple scheme for MP, the NOAH scheme for LS and the MRF scheme for PBL, show the worst performance.

Among the four sets of physical processes parameterizations, the largest impact of changing schemes on the prediction of precipitation magnitude and area comes from LS, while CU and MP mainly influence the corresponding prediction for heavy rainfall. Using CU is beneficial to forming light large-area rainfall, but not in favor of forming heavy local rainfall. Compared with the B-M-J scheme, both the SAS and K-F scheme produce heavy local rainfall more easily. For LS, the NOAH (SLAB) scheme tends to predict light large-area (heavy local) rainfall. Magnitude and area of precipitation predicted by the MRF scheme are similar to those with the YSU scheme. In terms of the three schemes for MP, WSM6 is most beneficial in producing heavy local rainfall, and next is NCEP3.

Variations of prediction resulting from changing schemes for LS and CU are very significant in both thermodynamics (such as CAPE and humidity) and dynamics (such as low-level jet and wind convergence at lower levels) variables; whereas, prominent variations caused by changing schemes for MP is concentrated in dynamics variables. Low-level jet and humidity concentration are both stronger, accompanied by more convective precipitation, with the combination of the SAS or K-F, WSM6, SLAB and YSU scheme than with the other combinations. When MP is with Simple, LS with SLAB and PBL with MRF, CAPE is stronger. In addition, turning CU off leads to the domination of stratiform rain in the precipitation process and the enhancement of impact of eddy vertical transport in PBL on precipitation.

For the NWP of AFRS, only by selecting appropriate combinations of parameterization schemes, as well as reasonably describing the physical processes related to heavy rainfall, such as wind convergence at lower levels and latent-heat release for condensation, vertical transport of heat and moisture and conversion among different hydrometeors, thereby rationally depicting the multi-scale interactions associated with heavy rainfall among low-level jet at synoptic scale and MCS, can its performance be improved effectively. In terms of the AFRS case in this study, the combination of the NCEP3 scheme for MP, the YSU scheme for PBL, the SLAB scheme for LS and the SAS scheme for CU gives the prediction of precipitation closet to observations, while that of the Simple, MRF, NOAH and B-M-J (or no cumulus option) scheme for MP, PBL, LS and CU respectively gives the prediction of precipitation furthest from observations. It should be noted that, the combination of different schemes for different parameterizations with the best performance of precipitation prediction is achieved based on only one case. Therefore, more experiments on NWP of AFRS are needed in future work to verify the universality of this combination, thereby to achieve proper combination of different parameterization schemes for NWP of AFRS.

REFERENCES:

[1] SUN Jian-hua, ZHAO Si-xiong. A diagnosis and simulation study of a strong heavy rainfall in South China [J]. Chin J Atmos Sci, 2000, 24(3): 381-392 (in Chinese).

[2] MENG Wei-guang, WANG An-yu, LI Jiang-nan, et al. Multi-MCSs (Mesoscale Convective Systems) over the heavy rainfall region during 23-24 May 1998 in South China [J]. J Sun Yat-sen Univ (in Chinese), 2003, 42(3): 73-77.

[3] ZHANG Xiao-hui, NI Yun-qi. A comparative study of a frontal and a non-frontal convective systems [J]. Acta Meteorol Sinica, 2009, 67(1): 108-121 (in Chinese).

[4] ZHANG Xu-bin, ZHANG Yi. Numerical simu lation of a heavy rainfall event in southern China: the mechanism of mesoscale convective system genesis and development [J]. Sci Meteorol Sinica, 2011, 31(2): 145-152 (in Chinese).

[5] LIU Shu-yuan, ZHENG Yong-guang, TAO Zu-yu. The analysis of the relationship between pulse of LLJ and heavy rain using wind profiler data [J]. J Trop Meteorol, 2003, 9(2): 158-163.

[6] HE Bian, SUN Zhao-bo. Diagnostic analysis and numerical simulation of persistent torrential rain in South China in June 2008 [J]. Sci Meteorol Sinica, 2010, 30(2): 164-171 (in Chinese).
[7] CHEN Hong, ZHAO Si-xiong. Heavy rainfall in South China and related circulation during first GARP global experiment period [J]. Chin J Atmos Sci, 2000, 24(2): 238-252 (in Chinese).
[8] SUN Jian, ZHAO Ping, ZHOU Xiu-ji. The mesoscale structure of a South China rainstorm and the influence of complex topography [J]. Acta Meteorol Sinica, 2002, 60 (3): 333-342 (in Chinese).
[9] WANG Wei, SEAMAN N L. A comparison study of convective schemes in a mesoscale model [J]. Mon Wea Rev, 1997, 125(2): 252-278.
[10] GALLUS Jr. W A. Eta simulations of three extreme rainfall events: Impact of resolution and choice of convective scheme [J]. Wea Forecast, 1999, 14 (3): 405-426.
[11] GU Jian-feng. Comparative experiments on precipitation prediction with different deep convective parameterization scheme [J]. Meteorol Mon, 1999, 25(4): 39-44 (in Chinese).
[12] WANG Jian-jie, HU Xin, GUO Xiao-rong. Comparison experiments on cumulus parameterization schemes of the MM5 [J]. J Appl Meteorol Sci, 2001, 12 (1): 41-53 (in Chinese).
[13] WANG Chen-xi. Comparison experiments on the effects of different cumulus parameterization scheme in MM5 on precipitation [J]. Sci Meteorol Sinica, 2004, 24 (2): 168-176 (in Chinese).
[14] JANKOV I, GALLUS Jr. W A, SHAW B, KOCH S E. An Investigation of IHOP Convective System Predictability Using a Matrix of 19 WRF Members [C]// 84th AMS Annual Meeting, Seattle, U.S.A., Jan. 10-15, 2004.
[15] JANKOV I, GALLUS Jr. W A, SEGAL M, SHAW B, KOCH S E. The impact of different WRF model physical parameterizations and their interactions on warm season MCS rainfall [J]. Wea Forecast, 2005, 20 (6): 1 048-1 060.
[16] ZHANG Man, WANG Ang-sheng, JI Zhong-zhen. Influence of different precipitation parameterization schemes on a simulated "03.7" heavy rainfall case [J]. Chin J Atmos Sci, 2006, 30(3): 441-451 (in Chinese).
[17] XUE Gen-yuan, ZHANG Jian-hai, CHEN Hong-mei, et al. The comparisons of different convective parameterization schemes applying precipitation's forecast of typhoon landing on Zhejiang and Fujian provinces [J]. Plateau Meteorol, 2007, 26(4): 765-773 (in Chinese).
[18] WU Hong-yu, CHEN Dei-hui, XU Guo-qiang. Sensitive experiments of various parameterization schemes in different physical processes on Guizhou precipitation [J]. Meteorol Mon, 2007, 33(4): 23-28 (in Chinese).
[19] LI Yan, QIU Cong-jian, ZHANG Jian-guo. The comparative trial experiments with different convection parameterization schemes in mesoscale models [J]. J Trop Meteorol, 2008, 24(6): 609-618 (in Chinese).
[20] SUN Jing, LOU Xiao-feng, SHI Yue-qin. The effects of different microphysical schemes on the simulation of a meiyu front heavy rainfall [J]. Acta Meteorol Sinica, 2011, 69(5): 799-809 (in Chinese).
[21] LIAO Jing-biao, WANG Xue-mei, XIA Bei-cheng, et al. The effects of different physics and cumulus parameterization schemes in WRF on heavy rainfall simulation in PRD [J]. J Trop Meteorol, 2012, 28(4): 461-470 (in Chinese).
[22] ARAKAWA A, CHEN Jeng-ming. Closure assumptions in the cumulus parameterization problem [C]// Short and Medium Range Numerical Weather Prediction, MATSUNO T (ed), Tokyo, Japan. Aug. 4-8, 1986.
[23] MOLINARI J M, DUDEK M. Parameterization of convective precipitation in mesoscale numerical models: a critical review [J]. Mon Wea Rev, 1992, 120 (2): 326-344.
[24] HAMMARSTRAND U. Questions involving the use of traditional convection parameterization in NWP models with higher resolution [J]. Tellus, 1998, 50A(3): 265-282.
[25] XING Yu, LEE Tae-young. Role of convective parameterization in simulations of a convection band at grey-zone resolutions [J]. Tellus, 2010, 62A(5): 617-632.
[26] KUELL V, GASSMANN A, BOTT A. Towards a new hybrid cumulus parameterization schemes for use in non-hydrostatic weather prediction models [J]. Quart J Roy Meteorol Soc, 2007, 133(623): 479-490.
[27] DENG Ai-jun, STAUFFER D R. On improving 4-kmmesoscale model simulations [J]. J Appl Meteorol Climatol, 2006, 45(3): 361-381.
[28] KOTRONI V, LAGOUVARDOS K. Evaluation of MM5 high-resolution real-time forecasts over the urban area of Athens, Greece [J]. J Appl Meteorol, 2004, 43 (11): 1 666-1 678.
[29] NIEMELÄS, FORTELIUS C. Applicability of large-scale convection and condensation parameterization to meso-γ-scale HIRLAM: a case study of a convective event [J]. Mon Wea Rev, 2005, 133(8): 2 422-2 435.
[30] ARAKAWA A, SCHUBERT W H. Interaction of cumulus cloud ensemble with the large-scale environment. Part I [J]. J. Atmos. Sci., 1974, 31: 671-701.
[31] GRELL G A. Prognostic evaluation of assumptions used by cumulus parameterizations [J]. Mon Wea Rev, 1993, 121: 764-787.
[32] PAN Hua-lu, WU Wan-shu. Implementing a mass flux convection parameterization for the NMC Medium-Range Forecast model [R]. NMC note, 1995, 409: 40pp.
[33] HAN Jongil, PAN Hua-lu. Revision of convection and vertical diffusion schemes in the NCEP global forecast system [J]. Wea Forecast, 2011, 26(4): 520-533.
[34] BETTS A K. A new convective adjustment scheme. Part I: Observational and theoretical basis [J]. Quart J Roy Meteorol Soc, 1986, 112: 677-691.
[35] BETTS A K, MILLER M J. A new convective adjustment scheme. Part II: Single column tests using GATE wave, BOMEX, and arctic air-mass datasets [J]. Quart J Roy Meteorol Soc, 1986, 112: 693-709.
[36] JANJIC Z I. The step-mountain Eta coordinate model: further developments of the convection, viscous sublayer and turbulence closure schemes [J]. Mon Wea Rev, 1994, 122: 927-945.
[37] JANJIC Z I. Comments on "Development and Evaluation of a Convection Scheme for Use in Climate Models" [J]. J Atmos Sci, 2000, 57: p. 3686.

[38] KAIN J S, FRITSCH J M. A one-dimensional entraining/detraining plume model and its application in convective parameterization [J]. J Atmos Sci, 1990, 47: 2784-2802.
[39] KAIN J S, FRITSCH J M. Convective parameterization for mesoscale models: The Kain-Fritcsh scheme [C]// The Representation of Cumulus Convection in Numerical Models. Boston, MA: American Meteorological Society, 24: 165-170.
[40] LIN Yuh-lang, FARLEY R D, ORVILLE H D. Bulk parameterization of the snow field in a cloud model [J]. J Climate Appl Meteorol, 1983, 22: 1 065-1 092.
[41] HONG S Y, LIM J O J. The WRF Single-Moment 6-Class Microphysics Scheme (WSM6) [J]. J Kor Meteorol Soc, 2006, 42: 129-151.
[42] DUDHIA J, HONG S Y, LIM K S. A new method for representing mixed-phase particle fall speeds in bulk microphysics parameterizations [J]. J Meteorol Soc Jpn, 2008, 86A: 33-44.
[43] HONG S Y, JUANG H M H, ZHAO Qing-yun. Implementation of prognostic cloud scheme for a regional spectral model [J]. Mon Wea Rev, 1998, 126: 2 621-2 639.
[44] HONG S Y, DUDHIA J, CHEN Shu-hua. A Revised Approach to Ice Microphysical Processes for the Bulk Parameterization of Clouds and Precipitation [J]. Mon Wea Rev, 2004, 132: 103-120.
[45] HU Zhi-jin, LOU Xiao-feng, BAO Shao-wu, et al. A simplified explicit scheme of phase-mixed cloud and precipitation [J]. J Appl Meteorol Sci, 1998, 9 (3): 257-264 (in Chinese).
[46] LIU Qi-jun, HU Zhi-jin, ZHOU Xiu-ji. Explicit cloud schemes of HLAFS and simulation of heavy rainfall and clouds, Part I: explicit cloud schemes [J]. J Appl Meteorol Sci, 2003, 14 (suppl.): 60-67 (in Chinese).
[47] BLACKADAR A K. Modeling the nocturnal boundary layer [C]// Preprints, Third Symposium on Atmospheric Turbulence, Diffusion and Air Quality, Raleigh, NC, Amer Meteorol Soc, 1976: 46-49.
[48] BLACKADAR A K. High resolution models of the planetary boundary layer [M]// Advances in Environmental Science and Engineering, PFAFFLIN J, ZIEGLER E. (ed), Vol. 1, No. 1, Gordon and Breach, 50-85.
[49] DUDHIA J. A multi-layer soil temperature model for MM5 [C]// Sixth Annual PSU/NCAR Mesoscale Model Users' Workshop, Boulder CO, 1996: 49-50.
[50] CHEN Fei, DUDHIA J. Coupling an advanced land surface-hydrology model with the Penn State-NCAR MM5 modeling system. Part I: Model implementation and sensitivity [J]. Mon Wea Rev, 2001, 129: 569-585.
[51] EK M B, MITCHELL K E, LIN Y, et al. Implementation of Noah land surface model advances in the National Centers for Environmental Prediction operational mesoscale Eta model [J]. J Geophys Res, 2003, 108 (D22): 8-851.
[52] HONG S Y, PAN Hua-lu. Nonlocal boundary layer vertical diffusion in a medium-range forecast model [J]. Mon Wea Rev, 1996, 124: 2 322-2 339.
[53] HONG S Y, NOH Y, DUDHIA J. A new vertical diffusion package with an explicit treatment of entrainment processes [J]. Mon Wea Rev, 2006, 134: 2 318-2 341.
[54] HONG S Y. Stable Boundary Layer Mixing in a Vertical Diffusion Scheme [C]// Kor Meteorol Soc, Fall Conference, Seoul, 2007: 25-26.
[55] KUO Ying-hwa, CHENG Lin-sheng, ANTHES R A. Mesoscale analysis of the Sichuan flood catastrophe 11-15 July 1981 [J]. Mon Wea Rev, 1986, 114 (11): 1 984-2 003.
[56] YANAI M, ESBENSEN S, CHU J H. Determination of bulk properties of tropical cloud clusters from large-scale heat and moisture budgets [J]. J Atmos Sci, 1973, 30: 611-627.
[57] THOMPSON Jr. R M, PAYNE S W, RECKER E E, et al. Structure and properties of synoptic-scale wave disturbances in the Intertropical Convergence Zone of the eastern Atlantic [J]. J Atmos Sci, 1979, 36: 53-72.
[58] YANAI M, JOHNSON R H. Impacts of cumulus convection on thermodynamic fields [M]// Representation of Cumulus Convection in Numerical Models of the Atmosphere, Meteorol Monogr, No. 46, Amer Meteorol Soc, 1993: 39-62.
[59] LIAO Jie, TAN Zhe-min. Numerical simula tion of a heavy rainfall event along the Meiyu front: Influences of different scale weather systems [J]. Acta Meteorol Sinica, 2005, 63(5): 771-789 (in Chinese).

Citation: ZHANG Xu-bin, WAN Qi-lin, XUE Ji-shan, et al. The impact of different physical processes and their parameterizations on forecast of a heavy rainfall in South China in annually first raining season [J]. J Trop Meteorol, 2015, 21(2): 194-210.